

## Robust balance control of a one-legged, pneumatically-actuated, Acrobot-like hopping robot.

John Leavitt, James E. Bobrow, Athanasios Sideris,  
Department of Mechanical and Aerospace Engineering  
University of California, Irvine  
Irvine, CA 92697  
{leavittj, jebobrow, asideris}@uci.edu

**Abstract**— We investigate approaches to balance control of an under-actuated robot. The robot is similar in structure to the Acrobot, but it is actuated with a pneumatic cylinder rather than an electric motor, and it is capable of hopping. Regions of attraction of the control system are studied, and two methods are presented that increase the size of this region. One is a different mechanical design, and the other is a more robust control approach based on  $H_\infty$  methods. The result is a much improved balance controller for a hopping robot.

### I. INTRODUCTION

The focus of this paper is on the robust balance control of an underactuated hopping robot. Because we desire this robot to be inexpensive and simple to construct, as well as light and powerful, we have chosen to actuate it pneumatically. In addition to helping achieve these goals, pneumatic cylinders can store energy, making them ideal for hopping. One robot design that has potential as a hopping robot is an Acrobot [1] with its base link free to rotate, but unattached to the ground. The Acrobot has become a popular control problem for underactuated robotic systems. In its upright position, the Acrobot can be a model for a leg with a single knee actuator, and zero actuation at the ankle. Traditionally, while the robot is free to rotate about the ankle, the foot is fixed in space. The so-called swing-up control problem deals with bringing this leg (or gymnast [1]) from a hanging position to an inverted position.

Berkemeier and Fearing [5], as well as Miyazaki et al. [3] and Van de Panne [4], have studied the hopping Acrobot, in which the foot is free to rotate and unattached to the ground, and the robot maintains an upright position during stance phases. In this case the balancing control problem becomes difficult, because while Spong swings the robot to near equilibrium before activating his balancing controller, the hopping Acrobot must be able to maintain its upright position after landing with considerable kinetic energy.

Our first attempts at building and balancing an experimental Acrobot under disturbances were a failure. We found that under the control of a linear quadratic regulator (LQR), the Acrobot had very low stability margins, and the relatively slow dynamics of our pneumatic actuator exacerbated the problem. Work has been done

to achieve more effective balancing controllers than the LQR used by Spong (see [6],[2],[7],[9]), showing significant but nonetheless small improvement. Of the methods we tested, the robust control formulation of [6] seemed to perform the best, but it was still unsatisfactory. In particular, all of these controllers have small regions of attraction when applied to the nonlinear dynamics of the acrobot. In order to increase the stability margins, Zergeroğlu, et al. [7] have modified the Acrobot dynamics by adding a counterweight. Adding natural stability to the robot, the counterweight has the drawback that it must hang below the first link. In this paper we modify the Acrobot design to increase its stability while maintaining its feasibility as a hopping robot. In addition, we improve on the balance control design by using  $H_\infty$  methods to create a compensator that is robust to the nonlinearities of the system.

Our robot is essentially an Acrobot with a wheel fixed to the first link. Figure 1 shows one version of the experimental hardware. This model can be thought of as a person sitting on a rocking horse, influencing its motion by swinging their torso back and forth. As well as adding stability to the vertical balancing position, the wheel offers a wider range of non-vertical equilibrium points. These non-vertical positions are generally more stable and allow for an upward swing of the center of mass, making them better for a hopping robot.

### II. REGION OF ATTRACTION

In order to examine the performance of various control designs on the nonlinear system, we looked at their region of attraction around the vertical balance equilibrium point. We first used Spong's model, whose parameters are specified in Table 1 of [1]. To plot the four-dimensional region of attraction for the nonlinear system in two dimensions, we assumed that the two joint velocities were zero. We then simulated the system, starting from positions neighboring the equilibrium point. We terminated the simulation using the following criteria: 1. The robot's first link must converge to within 5 degrees of the equilibrium point within 20 seconds. 2. The robot's first link angle may not exceed  $\pm 720^\circ$ . For a given initial condition, if these criteria were not satisfied during the simulation, it was not included in the region of attraction



Fig. 1. The Robot

plot. Applying this criteria to the entire range of possible initial conditions, Spong's LQR ( $K = [-242.52 \ -96.33 \ -104.59 \ -49.05]$ ) yields the region of attraction shown in the top plot of Fig 2. To obtain this figure, points were tested on a grid of  $10^\circ$  spacing, with the stable points marked using a hollow diamond and the equilibrium point marked using a solid diamond.

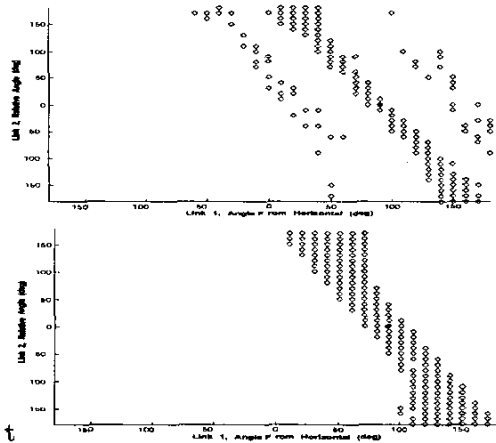


Fig. 2. Region of Attraction, Spong's Robot,  $K = [-242.52 \ -96.33 \ -104.59 \ -49.05]$  (top), and  $K = [-253.3632 \ -106.7316 \ -110.0362 \ -52.7513]$

Xin and Kaneda [6] have outlined a robust control approach to designing a linear compensator, which yields  $K = [-253.3632 \ -106.7316 \ -110.0362 \ -52.7513]$ . Again, using Spong's nonlinear model linearized around the vertical equilibrium point, we obtain the region of attraction shown in the bottom of Fig. 2. Note that the region of attraction is larger than that of the original compensator.

Next we examine a modified acrobot, with the same

parameters as before, but with the addition of a massless wheel whose rotation axis passes through first link, and whose contact point on the outer rim is the same as axis of rotation of joint 1 of the original Acrobot. (see Fig. 5). Using the LQR control approach of [1] on the new linearized system with  $Q$  and  $R$  matrices chosen to give feedback gains of similar magnitude, Fig. 3 shows the regions of attraction corresponding to wheels of radii  $r = 5/8$  meters and  $r = 11/16$  meters. Although not

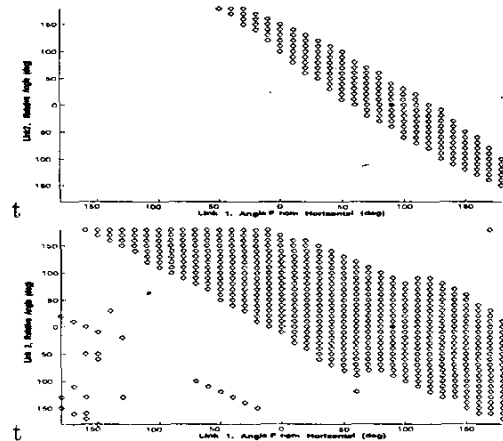


Fig. 3. Region of Attraction, Wheeled Acrobot,  $K = [196.9 \ 147.8 \ 119.4 \ 70.4]$ ,  $r = 5/8$  m (top) and  $K = [189.7 \ 154.4 \ 120.9 \ 73.9]$ ,  $r = 11/16$  m

shown, at  $r = 3/4$  meters the region of attraction fills the entire set of possible zero-velocity initial conditions. And while the region of attraction starts to increase significantly at around  $r = 5/8$  meters, we noticed that at smaller radii, the gain  $K$  decreases over constant  $Q$  and  $R$  (with increasing radius). The increasing region of attraction and decreasing gain with increasing radius leads us to the conclusion that a wheeled Acrobot is easier to balance than a comparable Acrobot. Having this evidence, we decided to implement a wheeled Acrobot using a pneumatic cylinder as an actuator.

### III. THE KINEMATICS OF THE ROBOT

As previously stated, the robot we built is powered by a pneumatic cylinder. Using pressure sensors we can control the force that air exerts on the piston (see Section VI). However, to implement a balance controller, it is helpful to convert from force on the piston to torque at the hinge. This can be accomplished easily by examining the kinematics of the linkage. Figure 4 shows a drawing of the linkage with right triangles overlaid. In the last two drawings, the pertinent lengths and angles are labelled. The triangle corresponding to link 2 is labelled ABC, with angles  $a$ ,  $b$ , and  $c$ . Similarly, link 1 is given triangle DEF with angles  $d$ ,  $e$ , and  $f$ .  $S$  is the full length of the

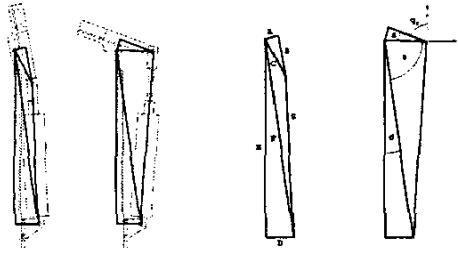


Fig. 4. Drawing of linkage (left), and geometric representation (right)

cylinder, and  $s$  is the corresponding angle shown.

$$\begin{aligned} a &= \tan^{-1} \left( \frac{A}{B} \right) \\ d &= \tan^{-1} \left( \frac{D}{E} \right) \\ d + s - a - q_2 &= 0 \\ s &= q_2 + a - d \\ S &= \sqrt{C^2 + F^2 - 2CF \cos s} \end{aligned} \quad (1)$$

Now to find the relationship between torque at the hinge and force on the piston, we equate the power exerted by each.

$$\begin{aligned} \tau_2 \dot{q}_2 &= F \dot{S} \\ \tau_2 &= J(q_2) F \end{aligned} \quad (2)$$

where  $J(q_2) = \frac{\dot{S}}{\dot{q}_2}$ .  $J$  may be found explicitly by differentiating (1).

$$\begin{aligned} 2S\dot{S} &= 2CF\dot{s} \sin s \\ \dot{S} &= \left( \frac{1}{S} CF \sin s \right) \dot{q}_2 \\ \Rightarrow J &= \frac{1}{S} CF \sin s \end{aligned} \quad (3)$$

#### IV. BALANCING LQR

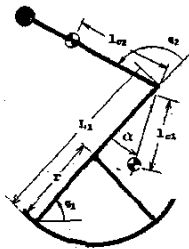


Fig. 5. Important dimensions of the robot

After obtaining a suitable force controller, and a good way of sensing the robot's state (see [10]), we turned our attention to obtaining a balance control law. Our approach relies on linear control techniques, which require that the model be linearized about various equilibrium points. Our model consists of two rigid links, with centers

of mass and moments of inertia determined experimentally. We obtained the centers of mass by fitting the equilibrium points of the model to the observed equilibrium points, using a nonlinear least-squares algorithm. In order to obtain the linearized model, the nonlinear equations of motion are first required.

Define  $\hat{i}$  and  $\hat{j}$  as unit vectors expressed in the fixed frame in the horizontal and vertical directions, respectively. The positions of the centers of mass of links 1 and 2,  $\mathbf{p}_1$  and  $\mathbf{p}_2$ , expressed in the fixed frame are

$$\begin{aligned} \mathbf{p}_1 &= [(L_1 - r) \cos(q_1) - l_{c1} \cos(q_1 + \alpha) - r q_1] \hat{i} \\ &\quad + [(L_1 - r) \sin(q_1) - l_{c1} \sin(q_1 + \alpha)] \hat{j} \\ \mathbf{p}_2 &= [(L_1 - r) \cos(q_1) + l_{c2} \cos(q_1 + q_2) - r q_1] \hat{i} \\ &\quad + [(L_1 - r) \sin(q_1) + l_{c2} \sin(q_1 + q_2)] \hat{j}. \end{aligned}$$

Differentiating  $\mathbf{p}_1$  and  $\mathbf{p}_2$ ,

$$\begin{aligned} \mathbf{v}_1 &\equiv \dot{\mathbf{p}}_1 = [-(L_1 - r) \sin(q_1) \dot{q}_1 + L_{c1} \sin(q_1 + \alpha) \dot{q}_1 - r \dot{q}_1] \hat{i} \\ &\quad + [(L_1 - r) \cos(q_1) \dot{q}_1 - L_{c1} \cos(q_1 + \alpha) \dot{q}_1] \hat{j} \\ \mathbf{v}_2 &\equiv \dot{\mathbf{p}}_2 = [-(L_1 - r) \sin(q_1) \dot{q}_1 - L_{c2} \sin(q_1 + q_2) (\dot{q}_1 + \dot{q}_2) - r \dot{q}_1] \hat{i} \\ &\quad + [L_1 \cos(q_1) \dot{q}_1 + l_{c2} \cos(q_1 + q_2) (\dot{q}_1 + \dot{q}_2) - r \cos(q_1) \dot{q}_1] \hat{j} \end{aligned}$$

From the position and velocity functions we obtain the kinetic and potential energy equations. Taking  $v_1^2 = \mathbf{v}_1^T \mathbf{v}_1$  and  $v_2^2 = \mathbf{v}_2^T \mathbf{v}_2$ ,

$$\begin{aligned} T &= (1/2)(m_1 v_1^2 + m_2 v_2^2 + I_1 \dot{q}_1^2 + I_2 (\dot{q}_1 + \dot{q}_2)^2) \\ V &= m_1 g [l_{c1} \sin(q_1)] + m_2 g [L_1 \sin(q_1) + l_{c2} \sin(q_1 + q_2)]. \end{aligned}$$

where  $I_1$  and  $I_2$  are the moment of inertia of links 1 and 2 about their mass centers, respectively.

Defining  $\mathbf{q} \equiv \begin{bmatrix} q_1 \\ q_2 \end{bmatrix}$  and application of Lagrange's equations to  $T - V$  for our system gives equations of the form

$$\mathbf{M} \ddot{\mathbf{q}} + \mathbf{h}(\mathbf{q}, \dot{\mathbf{q}}) = \boldsymbol{\tau}, \quad (4)$$

where  $\mathbf{M}$  is the usual mass matrix, and  $\mathbf{h}(\mathbf{q}, \dot{\mathbf{q}})$  is the remaining terms in Lagrange's Equations including forces due to gravity. The joint torque vector  $\boldsymbol{\tau} = \begin{bmatrix} 0 \\ \tau_2 \end{bmatrix}$ , represents zero torque at the first joint (it is unactuated) and torque  $\tau_2$  at the second joint.

The joint torque  $\tau_2$  is not a control signal since it results from gas flow into a cylinder. The differential equation for  $\tau_2$  can be obtained as follows. From (2),

$$\begin{aligned} \tau_2 &= J(q_2) F \\ \tau_2 &= J F + J \dot{F}. \end{aligned}$$

Using the feedback linearized force controller derived in Section VI,  $\dot{F} = -k_p(F - F_d)$ , where  $F_d$  is the desired cylinder force and  $k_p$  is a feedback gain, the above two equations yield the following first-order behavior for the torque actuator

$$\tau_2 = \tau_2 \left( \frac{J}{J - k_p} \right) + k_p u \quad (5)$$

where

$$J = CF \left( \frac{\dot{s} \cos s}{S} - \frac{\dot{S} \sin s}{S^2} \right),$$

and the control  $u$  is defined as  $u = J F_d$ .

It follows then that the nonlinear state space equations for the system take the form

$$\dot{\mathbf{x}} = \begin{bmatrix} \mathbf{M}^{-1} (\boldsymbol{\tau} - \mathbf{h}(\mathbf{q}, \dot{\mathbf{q}})) \\ \tau_2 \left( \frac{J}{J - k_p} \right) + k_p u \end{bmatrix},$$

where  $\mathbf{x} = [q_1^T, \dot{q}_1^T, \tau_2]^T$ .

Now our state equation can be linearized about an equilibrium point  $\mathbf{x}_0$  to obtain the state matrices,  $\mathbf{A}, \mathbf{B}, \mathbf{C}, \mathbf{D}$ .

$$\mathbf{A} = \left. \frac{\partial \dot{\mathbf{x}}}{\partial \mathbf{x}} \right|_{\mathbf{x}=\mathbf{x}_0}$$

$$\mathbf{B} = \left. \frac{\partial \dot{\mathbf{x}}}{\partial \mathbf{u}} \right|_{\mathbf{x}=\mathbf{x}_0}$$

For now we'll assume we have access to the full state and that  $\mathbf{y} = \Delta \mathbf{x}$ . This means that  $\mathbf{C}$  and  $\mathbf{D}$  will be identity and 0, respectively. The state equations are now of the form

$$\Delta \dot{\mathbf{x}} = \mathbf{A} \Delta \mathbf{x} + \mathbf{B} \Delta \mathbf{u}$$

$$\mathbf{y} = \Delta \mathbf{x}$$

Next we seek an optimal gain  $\mathbf{K}$  that minimizes the cost function  $\int_0^\infty \Delta \mathbf{x}^T \mathbf{Q} \Delta \mathbf{x} + R \Delta u^2 dt$ , for  $\mathbf{Q} \in \mathcal{R}^{5 \times 5}$ ,  $\mathbf{Q} = \mathbf{Q}^T \geq 0$ , and  $R \in \mathcal{R}$ ,  $R > 0$ . The closed-loop feedback system that results from  $\Delta \mathbf{u} = -\mathbf{K} \Delta \mathbf{x}$  is known as a linear quadratic regulator, or LQR.  $\mathbf{Q}$  and  $R$  define the relative importance of each state and control in the

cost function. We chose  $\mathbf{P} = \begin{pmatrix} 15 & 0 & 0 & 0 & 0 \\ 0 & 15 & 0 & 0 & 0 \\ 0 & 0 & 1 & 0 & 0 \\ 0 & 0 & 0 & 1 & 0 \\ 0 & 0 & 0 & 0 & 1 \end{pmatrix}$  and  $R = 0.1$ , resulting in  $\mathbf{K}$  matrices of [46.0 64.0 25.5 15.7 3.5], [49.0 68.6 25.2 16.0 3.7], and [50.8 71.1 25.1 16.1 3.8], corresponding to set points of  $q_1 = 30^\circ$ ,  $45^\circ$ , and  $60^\circ$ . The MATLAB function LQR will calculate  $\mathbf{K}$ .

## V. ROBUST CONTROL

A major drawback of the LQR approach is that our system is actually nonlinear, and at large deviations from the point of linearization, the controller is ineffective. Here we describe an  $H_\infty$  optimal controller that is more robust to perturbations (or uncertainties) in the linearized model, making the system in turn more robust to model nonlinearities. In addition, the robust control perspective will let us minimize the required bandwidth of our actuator. This will allow us to discard the state of the actuator in our model, since actuator dynamics are high-frequency, leaving four states in the model description.

We consider the elements of the  $\mathbf{A}$ ,  $\mathbf{B}$ ,  $\mathbf{C}$ , and  $\mathbf{D}$  state space matrices obtained through linearization at different equilibrium points to be uncertain elements and we will design a controller that is robust to these uncertainties. We linearized about a few of the positions between  $q_1 = 30^\circ$  and  $q_1 = 60^\circ$  (see Figure 6), and obtained matrices

$$\mathbf{A} = \begin{bmatrix} 0 & 0 & 1 & 0 \\ 0 & 0 & 0 & 1 \\ a & b & 0 & 0 \\ c & d & 0 & 0 \end{bmatrix}$$

and

$$\mathbf{B} = \begin{bmatrix} 0 \\ 0 \\ e \\ f \end{bmatrix}$$

whose elements vary as  $a = a_1 + a_2 \delta$ , ...,  $f = f_1 + f_2 \delta$  with  $\delta = -1$  to  $1$ , for a set of known constants  $\{a_1, \dots, f_1\}$ , and  $\{a_2, \dots, f_2\}$ .

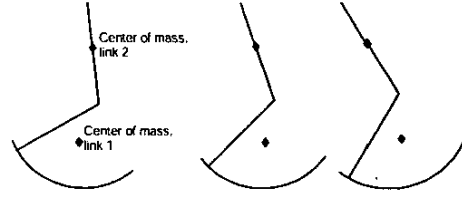


Fig. 6. Wheeled Acrobot balancing at 30, 45 and 60 degrees (angle of first link from horizontal)

Now

$$\Delta \dot{\mathbf{x}} = \mathbf{A} \Delta \mathbf{x} + \mathbf{B} \Delta \tau_2 + \begin{bmatrix} d_{b1} \\ d_{b2} \\ 0 \\ 0 \end{bmatrix}$$

where  $d_{b1}$  and  $d_{b2}$  are disturbances introduced to model initial perturbations in the joint angles from equilibrium. Written out,

$$\Delta \dot{\mathbf{x}} = \begin{bmatrix} \Delta x_3 + d_{b1} \\ \Delta x_4 + d_{b2} \\ a_1 \Delta x_1 + b_1 \Delta x_2 + c_1 \Delta \tau_2 + [a_2 \Delta x_1 + b_2 \Delta x_2 + c_2 \Delta \tau_2] \delta \\ c_1 \Delta x_1 + d_1 \Delta x_2 + f_1 \Delta \tau_2 + [c_2 \Delta x_1 + d_2 \Delta x_2 + f_2 \Delta \tau_2] \delta \end{bmatrix}$$

If we define

$$\begin{aligned} \zeta_1 &= a_2 \Delta x_1 + b_2 \Delta x_2 + c_2 \Delta \tau_2 \\ \zeta_2 &= c_2 \Delta x_1 + d_2 \Delta x_2 + f_2 \Delta \tau_2 \\ \xi_1 &= \zeta_1 \delta \\ \xi_2 &= \zeta_2 \delta \end{aligned}$$

then

$$\dot{\mathbf{x}} = \begin{bmatrix} \Delta x_3 + d_{b1} \\ \Delta x_4 + d_{b2} \\ a_1 \Delta x_1 + b_1 \Delta x_2 + c_1 \Delta \tau_2 + \xi_1 \\ c_1 \Delta x_1 + d_1 \Delta x_2 + f_1 \Delta \tau_2 + \xi_2 \end{bmatrix}$$

The output of our system is  $\mathbf{y} = \begin{bmatrix} \Delta x_1 + n_1 \\ \Delta x_2 + n_2 \\ \Delta x_3 + n_3 \\ \Delta x_4 + n_4 \end{bmatrix}$ , where  $n_k$ ,  $k = 1, 2, 3, 4$  are noise signals applied at each sensor and used to limit controller bandwidth.

We next define extended input and output vectors,  $\mathbf{W}$  and  $\mathbf{V}$ , defined as

$$\mathbf{W} = [\xi_1 \ \xi_2 \ d_{b1} \ d_{b2} \ n_1 \ n_2 \ n_3 \ n_4 \ \Delta \tau_2]^T$$

$\mathbf{V} = [z_1 \ z_2 \ z_3 \ y_1 \ y_2 \ y_3 \ y_4]^T$ . The signals  $z_1$ ,  $z_2$ , and  $z_3$  are the signals that will be used to measure how well our controller performs. In this case we let  $z_1$ ,  $z_2$ , and  $z_3$  be  $\Delta x_1$ ,  $\Delta x_2$ , and  $\Delta \tau_2$  respectively.

Now we can express the transfer matrix  $\mathbf{P}(s)$  which satisfies  $\mathbf{V}(s) = \mathbf{P}(s) \cdot \mathbf{X}(s)$ , using the standard notation

$\mathbf{P} = \begin{bmatrix} \mathbf{A} & \mathbf{B} \\ \mathbf{C} & \mathbf{D} \end{bmatrix}$  to denote the  $\mathbf{A}$ ,  $\mathbf{B}$ ,  $\mathbf{C}$ , and  $\mathbf{D}$  matrices

of a state space realization for it. Specifically,  $\mathbf{P} =$

	$\Delta x_1$	$\Delta x_2$	$\Delta x_3$	$\Delta x_4$	$\xi_1$	$\xi_2$	$d_{b1}$	$d_{b2}$	$n_1$	$n_2$	$n_3$	$n_4$	$\Delta \tau_2$
$\Delta x_1$	0	0	1	0	0	0	0	1	0	0	0	0	0
$\Delta x_2$	0	0	0	1	0	0	0	0	1	0	0	0	0
$\Delta x_3$	$a_1$	$b_1$	0	0	1	0	0	0	0	0	0	0	$e_1$
$\Delta x_4$	$c_1$	$d_1$	0	0	0	1	0	0	0	0	0	0	$f_1$
$\zeta_1$	$a_2$	$b_2$	0	0	0	0	0	0	0	0	0	0	$e_2$
$\zeta_2$	$c_2$	$d_2$	0	0	0	0	0	0	0	0	0	0	$f_2$
$y_1$	1	0	0	0	0	0	0	0	0	0	0	0	0
$y_2$	0	1	0	0	0	0	0	0	0	0	0	0	0
$y_3$	0	0	1	0	0	0	0	0	0	1	0	0	0
$y_4$	0	0	0	1	0	0	0	0	0	0	1	0	0

We have included labels on the rows and columns of the matrix for the sake of readability.

Next, we consider filters that are applied to the performance variables  $z_1$ ,  $z_2$ , and  $z_3$ . These filters will define the

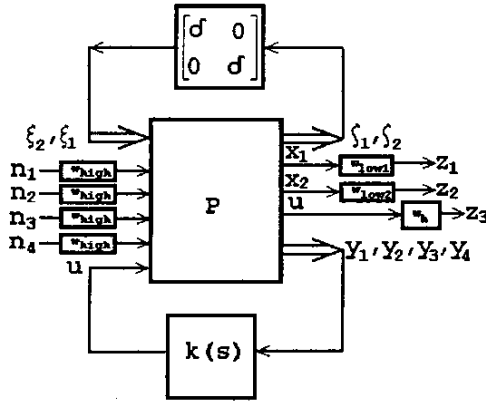


Fig. 7.  $H_\infty$  Optimal Control Framework

range of frequencies that we want our system to perform well in. For the variables  $\Delta x_1$  and  $\Delta x_2$  we define butterworth low-pass filters  $w_{low1}(s)$  and  $w_{low2}(s)$  with cutoff frequencies,  $f_{c1}$  and  $f_{c2}$ . These filters simply take into account the actual bandwidth of the system. Our control variable,  $\Delta \tau_2$ , is passed through a high-pass butterworth filter  $w_h(s)$  with cutoff frequency  $f_h$ . This is the filter which helps to penalize higher bandwidth controllers, since we only look at the high-frequency component of the control signal. The final filter is  $w_{high}$ , a high-pass filter that is applied to the four noise inputs. This comes from the assumption that the noise on our four signals is high-frequency noise, which adds no steady-state offset. We next obtain the controller from  $y(\equiv \Delta x)$  to  $\Delta \tau_2$  that minimizes the  $H_\infty$  norm between the remaining variables in  $W$  and  $V$ . The controller is first tested on the nonlinear simulation and eventually applied on the real system to verify that indeed works. By tuning various design parameters, such as  $f_{c1}$ ,  $f_{c2}$ , and  $f_h$ , and repeating the process, we obtained a robust controller with satisfactory performance as further discussed in Section VII.

## VI. FEEDBACK LINEARIZATION OF THE PNEUMATIC TORQUE CONTROL SUBSYSTEM

The LQR and robust controller discussed both take joint torque as the input. As we have stated, in order to control this torque, we must control the force that air exerts on the piston. Since the actual input was servovalve flow, we needed to design a fast inner feedback loop that provided the torque or force required required by either the LQR or the robust control compensators. This in turn requires that the pressure difference across each side of the actuator piston be sensed and controlled.

The following are steps to obtaining the force controller: Referring to Fig. 8,  $A$  is the area of the piston,

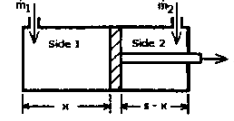


Fig. 8. Pneumatic Piston

with  $A_0$  being the area of the rod.  $P$  refers to pressure, with  $P_0$  being atmospheric pressure, and  $V$  is volume with  $V_0$  being the volume of the plumbing outside the cylinder. Flow rate is  $\dot{m}$ , and  $x$  is the piston position, which varies from 0 to  $s$ . The subscripts 1 and 2 refer to Sides 1 and 2.

Assuming air is an ideal gas, we refer to Bobrow and McDonell's derivation of rate of pressure in a pneumatic cylinder [11].

$$\dot{P}_1 = k \left( \frac{\dot{m}_1 RT}{V_1} - \frac{P_1 \dot{V}_1}{V_1} \right) \quad (6)$$

Similarly,

$$\dot{P}_2 = k \left( \frac{\dot{m}_2 RT}{V_2} - \frac{P_2 \dot{V}_2}{V_2} \right) \quad (7)$$

where  $k = \left( \frac{c_p}{c_v} \right) = 1.4$ . In terms of piston position  $x$ ,

$$\begin{aligned} V_1 &= A_1 x + V_{10} \\ V_2 &= A_2 (s - x) + V_{20} \\ \dot{V}_1 &= A_1 \dot{x} \\ \dot{V}_2 &= -A_2 \dot{x} \end{aligned}$$

Also assume:

$$\begin{aligned} \dot{m}_1 &= c_1 u \\ \dot{m}_2 &= -c_1 u \end{aligned} \quad (8)$$

where  $u$  is the servo-valve input and  $c_1$  is the associated valve constant. Using this information we can express  $\dot{F}$ , the force on the piston differentiated once, as

$$\dot{F} = k_1 u \left( \frac{A_1 V_2 + A_2 V_1}{V_1 V_2} \right) + \sigma(x, \dot{x}) \quad (9)$$

where

$$\sigma(x, \dot{x}) = -k \frac{P_1 \dot{V}_1 A_1}{V_1} + k \frac{P_2 \dot{V}_2 A_2}{V_2}$$

and

$$k_1 = kRTc_1$$

Now let  $e = F - F_d$  where  $F_d$  is the desired force. Assuming that our controller behaves as follows,

$$\dot{F} = -k_p e + \dot{F}_d \quad (10)$$

and assuming that  $\dot{F}_d = 0$ , and setting  $k_v = \frac{k}{k_1}$  and renaming  $k_p = \frac{k_p}{k_1}$ , we can obtain the control law,  $u =$

$$\left[ -k_p (P_1 A_1 - P_2 A_2 - P_0 A_0 - F_d) + k_v \left( \frac{P_1 V_1 A_1}{V_1} - \frac{P_2 V_2 A_2}{V_2} \right) \right] k_g(x) \quad (11)$$

where  $k_g(x) = \left( \frac{V_1 V_2}{A_1 V_2 + A_2 V_1} \right)$ . Because our valve input  $u$  is approximately proportional to the valve current, (11) may be fed into a current controller.  $k_p$  and  $k_v$  are essentially tunable parameters ( $\geq 0$ ). Note from (10) that  $k_p$  directly governs the response time of the force

control subsystem. The constant  $k_v$  in (11) governs the feed-forward control due to motion of the piston. It can be set experimentally by setting  $F_d = 0$ , and manually moving the piston sinusoidally, and adjusting  $k_v$  until the amplitude of the resulting sinusoidal force on the piston is minimized. The term  $k_g$  in (11) is essentially a nonlinear loop gain that varies as the piston position  $x$ . Note that  $k_g(x)$  is a minimum at the ends and a maximum near the cylinder's mid-stroke position. After some tuning of these gains, we were able to achieve a bandwidth of about 10 Hz. for this force control subsystem.

## VII. RESULTS

### A. Balancing LQR

For our experimental results we manually perturbed the system from its equilibrium point and observed the response. If the system quickly returned to this equilibrium point, it was called "good". We experimented with LQR controllers for both the five state model discussed and a four state model, which ignored the actuator dynamics. Both produced good results, as can be seen in Figure 9 (a) and (b). For the five state LQR, we turned  $k_p$  down significantly from the four state model. The purpose for this was to show that the model of the actuator dynamics could be used to compensate for a slow inner force control loop. The four state LQR took advantage of a fast inner force control loop, and we were able to get acceptable performance. As we stated before, the five state LQR for the set point  $q_1 = 45^\circ$  had for K the value [49.0 68.6 25.2 16.0 3.7]. This K gives a control torque in the units of Nm, and assumes the states are in units of rad, rad/s, and Nm. The four state LQR has for K values [11.93 17.26 6.58 4.0716], with the same units.

### B. Robust Control

The best controller we were able to find, in terms of performance and stability, was the robust controller. The controller we used has a 19th order state space representation before any model reduction was attempted. The results of perturbing the system with this controller are shown in 9 (c).

## VIII. CONCLUSION

We studied the regions of attraction of various control laws on the Acrobot system and found them unacceptably small for balance control using pneumatic actuators. We developed a feedback linearizing inner torque control system for the pneumatic actuator, and included these dynamics in the control design. We then added a circular arc to the bottom of the Acrobot to increase its region of attraction for balance control. The resulting robot has nice balance control characteristics and is capable of hopping. The pneumatic actuator is

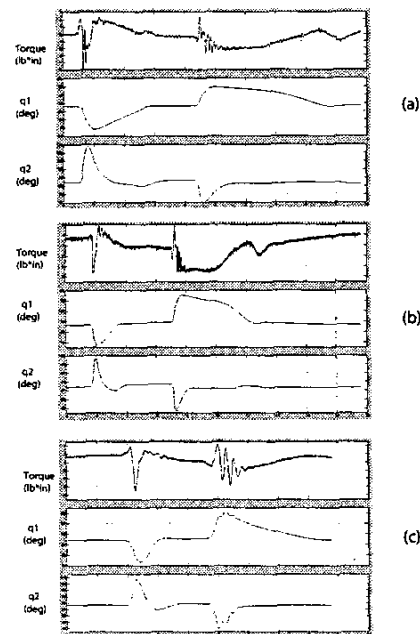


Fig. 9. Three Balance Control Laws. All plots are versus time (dependent axis), with each major division representing 1 second. Plots show the result of perturbing the robot by hand and allowing it to return to equilibrium. (a) LQR, 5 state model. (b) LQR, 4 state model. (c) Robust Controller, 4 state model

light-weight and is capable of delivering high power levels.

## IX. REFERENCES

- [1] Spong, M.: 1995, "The swing up control problem for the Acrobot," *Control Systems Magazine*, IEEE, Volume: 15 Issue: 1, Feb. 1995 Page(s): 49-55
- [2] Swing-up and balancing control of acrobot Kobayashi, T.; Kamine, T.; Suzuki, S.; Iwase, M.; Furuta, K.; SICE 2002, Proceedings of the 41st SICE Annual Conference, Volume: 5, 5-7 Aug. 2002 Page(s): 3072-3075
- [3] Miyazaki M. Sempel M. Koga M. Takahashi A., "A control of underactuated hopping gait systems: acrobot example," *Proceedings of the 39th IEEE Conference on Decision and Control*, Vol. 5, 2000, pp. 4797-802, Piscataway, NJ, USA.
- [4] "Towards agile animated characters" van de Panne, M.; Lasezlo, J.; Huang, P.; Faloutsos, P.; Robotics and Automation, 2000, Proceedings. ICRA '00. IEEE International Conference on, Volume: 1, 24-28 April 2000 Page(s): 682-687 vol. 1
- [5] Tracking fast inverted trajectories of the underactuated Acrobot Berkelemer, M.D.; Fearing, R.S.; Robotics and Automation, IEEE Transactions on, Volume: 15 Issue: 4, Aug. 1999 Page(s): 740-750
- [6] A robust control approach to the swing up control problem for the Acrobot Xin Xin; Kaneda, M.; Intelligent Robots and Systems, 2001, Proceedings. 2001 IEEE/RSJ International Conference on, Volume: 3, 29 Oct.-3 Nov. 2001 Page(s): 1650-1655 vol. 3
- [7] Lyapunov-based set-point control of the Acrobot Zergoglu, E.; Dixon, W.E.; Dawson, D.M.; Jaffar, S.; Hannan, M.W.; Proceedings of the 1998 IEEE International Conference on Control Applications, Volume: 2, 1-4 Sept. 1998 Page(s): 887-891 vol. 2
- [8] Enlarge your region of attraction using high-gain feedback Davidson, D.E.; Bortoff, S.A.; Decision and Control, 1994., Proceedings of the 33rd IEEE Conference on, Volume: 1, 14-16 Dec. 1994 Page(s): 634-639 vol. 1
- [9] Fuzzy control strategy for Acrobots combining model-free and model-based control Lai, X.; She, J.-H.; Ohyanis, Y.; Cai, Z.; Control Theory and Applications, IEE Proceedings-, Volume: 148 Issue: 6, Nov. 1999 Page(s): 505-510
- [10] J. Lovitt and A. Sideris and J.E. Bobrow, "High Bandwidth Tilt Measurement Using Low Cost Sensors", (Publication pending), University of California, Irvine, 2003.
- [11] James E. Bobrow and Brian W. McDonell, "Modeling, Identification, and Control of a Pneumatically Actuated, Force Controllable Robot," *IEEE Transactions on Robotics and Automation*, Vol. 14, No. 5, pp. 732-742, October 1998.
- [12] T. Kimura, S.Hara, T.Fujita, and T.Kagawa, Control for pneumatic actuator systems using feedback linearization with disturbance rejection, Proc. 1995 Amer. Contr. Conf. Seattle, WA, pp. 825-829, June 1995.